Check for updates

ADVANCED FUNCTIONAL MATERIALS
www.afm-journal.de

Light-Regulated Capillary Force Self-Assembly of Nano-Printed Pillars for Chiroptical Metamaterials

Sizhu Wu, Xinkai Li, Xin Liu, Haijian Hu, Rui Dong, Jincheng Ni, Deng Pan, Yanlei Hu, Chenchu Zhang, Chao Chen, Yachao Zhang, Haojie Xia, Dong Wu, and Zhaoxin Lao**

Capillary force self-assembly (CFSA) technology unfolds great potential in the fabrication of functional micro/nanostructures. To date, most self-assembly methods focus on monolithic microstructure manipulation yet it remains a challenge to achieve precise localized control over the CFSA process of micro/nanostructures. Herein, a light-regulated CFSA is proposed to realize the localized precise control of microstructures, leveraging on the synergistic effect of photothermally-responsive hydrogel and self-assembly technique. The micropillars with asymmetric cross-linking densities can readily prepare by applying a rationally designed laser and laser-exposing dosage, thereby realizing the on-demand steering of their bending directions. Significantly, owing to the giant capillary force deriving from the evaporating water, above micropillars can successfully assemble into highly-ordered chiral structures. Simulation coupling with fundamental hydrodynamics enables to shed light on the light steering principle over pillar's actuations. Last, on the basis of vortical dichroism spectra analysis, the chiral characteristics of light-regulated self-assembly including the chiral as well as the achiral self-assembled microstructures are successfully deployed. This strategy provides an avenue for fabricating the localized controllable self-assembly at the microscale and will bloom the field over metamaterials, microsensors, chiral optics, and so on.

1. Introduction

Self-assembly is a pervasive phenomenon in nature, referring to the spontaneous assembly of molecules, atoms, or micro/nanostructures into specific configurations or patterns under the influence of microscopic forces such as physical, chemical, or biological forces.[1] As a potent tool to manufacture ordered structures from nanoscale to macroscopic scale, self-assembly methods have obtained extensive research.[2] Currently, driving forces of self-assembly mainly include electrostatic forces, hydrogen bonding, van der Waals forces,[3] surface tension, capillary forces[4] and so on. Notably, capillary force self-assembly has garnered tremendous attention due to its prominent advantages such as low cost, simplicity, and scalability.[5,6]

Capillary forces are ubiquitously present in nature, and structures at the micro/nanoscale are more susceptible to capillary forces, for which capillary forces can be utilized for the fabrication of complex self-assembled microarchitectures.[7] Currently, CFSA has been reported widespread applications in building micro/nanoscale functional structures.[8] Researchers have developed a wide range of intriguing outcomes through CFSA techniques. Duan achieved controllable folding self-assemblies by independently manipulating collapse directions of micro/nanostructures through asymmetric cross-sections, curvature, and tilt angles.[9] Wu utilized multi-beam

S. Wu, X. Li, X. Liu, H. Hu, R. Dong, Y. Zhang, H. Xia, Z. Lao
Anhui Province Key Laboratory of Measuring Theory and Precision Instrument
School of Instrument Science and Optoelectronics Engineering
Hefei University of Technology
Hefei 230009, China
E-mail: laozx@hfut.edu.cn

J. Ni, Y. Hu, D. Wu
CAS Key Laboratory of Mechanical Behavior and Design of Materials
Department of Precision Machinery and Precision Instrumentation
University of Science and Technology of China
Hefei 230027, China

D. Pan
Information Materials and Intelligent Sensing Laboratory of Anhui Province
Anhui University
Hefei 230601, China

C. Zhang
Institute of Industry and Equipment Technology
Hefei University of Technology
Hefei 230009, China

C. Chen
Department of Materials Physics and New Energy Device
School of Materials Science and Engineering
Hefei University of Technology
Hefei 230009, China
E-mail: chaoc11@ustc.edu.cn

The ORCID identification number(s) for the author(s) of this article can be found under https://doi.org/10.1002/adfm.202407232

DOI: 10.1002/adfm.202407232

 © 2024 Wiley-VCH GmbH

16163028, 2024, 44, Downloaded from https://onlinelibrary.wiley.com/doi/10.1002/adfm.202407232 by University Of Science, Wiley Online Library on [02/01/2025]. See the Terms and Conditions (https://onlinelibrary.wiley.com/terms-and-conditions) on Wiley Online Library for rules of use; OA articles are governed by the applicable Creative Commons License

laser interference to develop micropillars, which are assembled into three-dimensional structures due to the dominant capillary force, enabling the rapid construction of large-area, controllable microstructures.[10] Hu reported controllable self-assemblies through intentionally breaking the intrinsic symmetry of the unit cells with synergistic effects of geometry and spatial arrangements of the micropillars.[11] Li utilized the evaporation process between liquid and polymers to achieve rapid and reversible modular transformation of microstructures with tunable topologies.[6] This strategy is broadly applicable to various geometric shapes and materials. However, in general, once assembled, these structures are typically in a fixed state and can hardly be adjusted or changed, resulting in limited flexibility and tunability.[5] In the process of CFSA, it is possible to accomplish designable bending deformation by modulating capillary forces, thereby achieving multifunctional structures. For instance, by tilting the substrate during the evaporation process, asymmetric capillary force distribution can be created, facilitating anisotropic self-assembly of micropillar arrays.[12] Additionally, processing the samples on a flexible substrate and then stretching the substrate to different degrees allow for variable assembly morphologies of the same structure.[13] However, due to the lack of inherent tunability in the structure itself, once the microstructure is programmed, the achievable functions and application fields of the self-assembled structures become constrained.

In recent years, dynamic controlling methods have attracted widespread research interest in developing localized tunable functional micro/nanostructures, which unfolds significant possibilities in the fabrication of microsensors and metamaterials.[14,15] For instance, in the fields of micro/nanoactuators and soft robotics, precise control over multiple joints enables the realization of various reconfigurable deformation modes in micromachines, which facilitates multifunctional operations in complex environments.[16] Owing to the stimuli-responsive properties of hydrogels, controllable structural changes can be achieved by adjusting external factors[17] such as temperature,[18] pH,[19,20] the magnetic field[21] and so on. Moreover, it is reported that self-assembly morphologies of the same laser-fabricated micropillars alter with the concentration of active solvents in the solution.[22,23] However, these efforts primarily focus on global structural manipulation and thus it remains a great challenge to achieve precise localized control over the capillary-assisted self-assembly process of micro/nanostructures. As an efficient methodology, the localized controlling method enables a flexible manipulation of functional microstructures, playing a significant role in the fields of microsensors and metamaterials.[24]

Among various external stimuli-responsive strategies, light regulating presents a highly promising solution[25,26] due to its outstanding intrinsic features, including remote operation, non-contact manipulation,[27] rapid responsiveness, and programmability.[28,29] This work provides a light-regulated CFSA strategy to realize localized manipulation of microstructures, which is based on the synergistic effect of tunable thermally-responsive hydrogels and self-assembly techniques. Using fs-laser direct writing, the photothermally-responsive micropillars with asymmetric cross-linking densities are fabricated, allowing for controllable bending directions, and then are self-assembled into ordered chiral structures via the capillary force in an evaporating liquid. Through synergistic control of the geometric shape and spatial topology of micropillars, the light-regulated self-assemblies have realized different chiral microstructures. By regulating laser processing parameters and light irradiance intensity, this research has successfully developed a photothermally-responsive micro-deformer that is able to achieve controllable deformation effectively. Subsequently, these tiny deformations lead to anisotropic capillary force between micropillars, which will enlarge these deformations in the consequent process of self-assembly and result in chiral microstructures. Lastly, according to the analysis of vortical dichroism (VD) spectra, the chiral characteristics of light-regulating self-assembled microstructures are demonstrated, showcasing the distinction between chiral and achiral self-assembled microstructures. This strategy provides an avenue for fabricating the localized controllable self-assembly at the microscale and would bloom the field over metamaterials, microsensors, chiral optics, and so on.

2. Results and Discussion

As depicted in **Figure 1a**, a fs-laser beam is focused into the photothermally-responsive hydrogel to readily fabricate the micropillars. The individual hydrogel monomers tend to form growing chains at the laser beam focus (Figure 1b), and the hydrogel cross-linking degrees are adjusted to laser scanning point step (SPS). Upon completion of the processing, samples are developed in ethanol for 5 min to remove the unpolymerized material, resulting in printed three-dimensional micropillars. Subsequently, the micropillars will enable guided bending when immersed in warm water (55 °C).[30]

The switchable temperature-induced deformation of the photothermally-responsive hydrogel is shown in Figure 1d. Variations of temperature have an impact on the interaction between hydrogel functional groups and water molecules, thus altering pores of the hydrogel, which results in volume contraction or expansion. When the ambient temperature exceeds the critical temperature (T_C), the hydrogen bonding between hydrophilic groups and water molecules weakens, while interactions among hydrophobic groups strengthen, bringing about the contraction of the hydrogel. Conversely, with the environmental temperature below T_C, strengthened hydrogen bonding makes the hydrogel expand.[31]

In order to further understand the deformation of laser-fabricated functional structures, we have employed a disc-shaped structure (diameter $L \approx 20$ μm, thickness $d \approx 3$ μm) as a reference model to investigate the expansion and contraction properties. To prevent the substrate adhesion from hindering the full deformation of microstructures, a connecting pillar, 10 μm in height, was designed between the disc-shaped structure and the substrate. With the hydrogel disc in a partially suspended state, it enables apparent observation of hydrogel deformation under variable ambient temperatures. When put into deionized water at 20 °C, the disc-shaped structure expands during the swelling process. Subsequently, it undergoes rapid shrinkage after being placed in deionized water at 55 °C (Figure 1b; Video S1, Supporting Information).

The deformability of hydrogels is typically associated with the cross-linking degree. As the density of cross-linking increases, the structure becomes more compact, which results in relatively

 © 2024 Wiley-VCH GmbH

16163028, 2024, 44, Downloaded from https://onlinelibrary.wiley.com/doi/10.1002/adfm.202407232 by University Of Science, Wiley Online Library on [02/01/2025]. See the Terms and Conditions (https://onlinelibrary.wiley.com/terms-and-conditions) on Wiley Online Library for rules of use; OA articles are governed by the applicable Creative Commons License

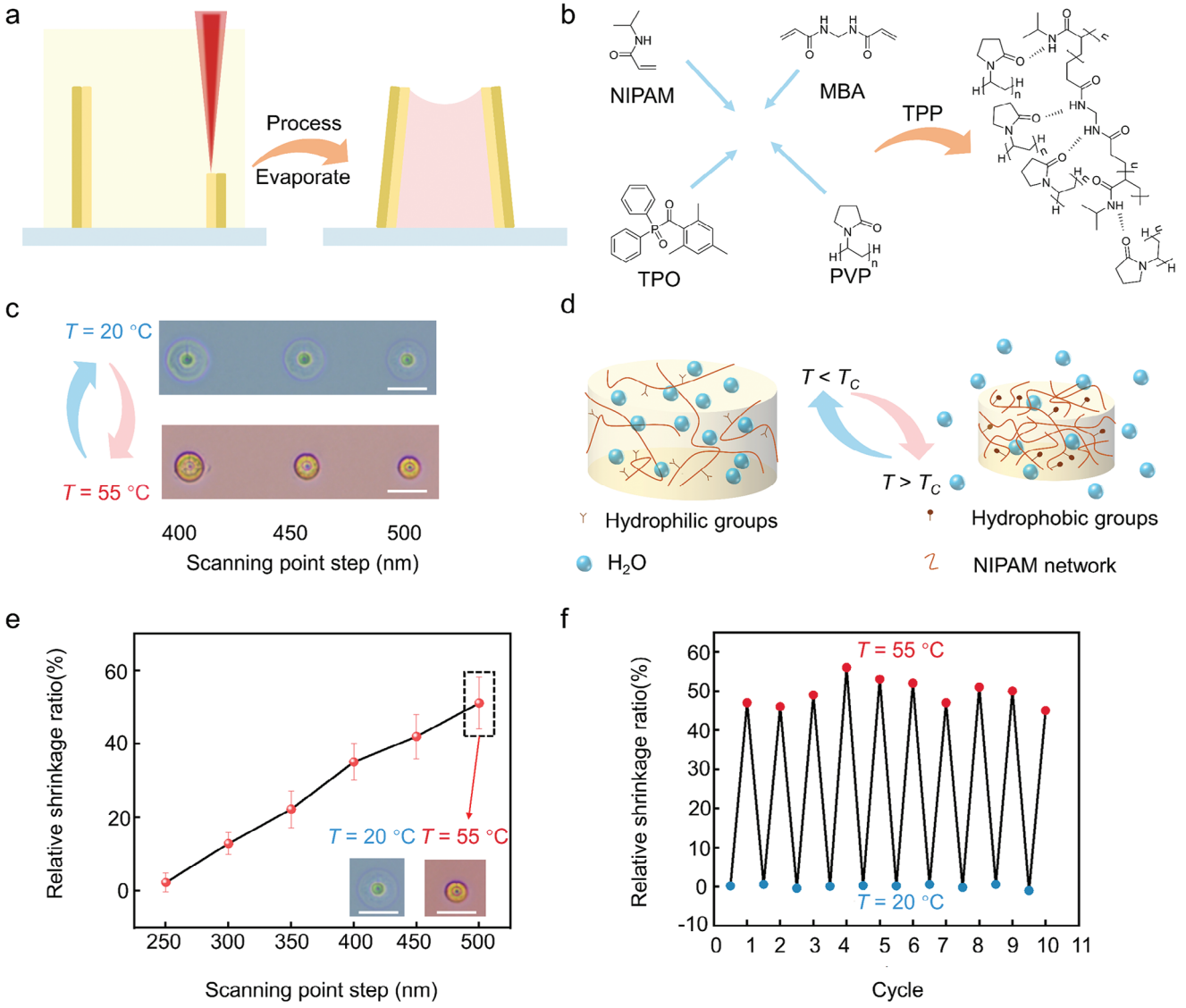

Figure 1. Basic performance analysis of photothermally-responsive hydrogel. a) Laser printing is employed to fabricate the photothermally-responsive hydrogel for constructing micropillars. The micropillars comprise two sections with distinctive cross-linking densities, where low and high cross-linking densities are represented by yellow and dark yellow, respectively. b) Components of temperature-sensitive hydrogels, including polymerizable monomers (N-Isopropyl acrylamide, NIPAM), crosslinkers (Methylene-Bis-Acrylamide, MBA), and photoinitiators (Diphenyl (2,4,6-trimethyl benzoyl) phosphine oxide, TPO). TPP represents two-photon polymerization. c) The hydrogel disc with expansion and contraction at 20 and 50 °C respectively. d) Temperature response principle of the hydrogel. e) The quantitative relationship between the SPS of laser processing and the relative shrinkage of the hydrogel disc. f) Repeatability verification of the hydrogel disc with an SPS of 500 nm at 20 and 55 °C. Scale bars: 10 μm.

weaker deformability of the hydrogel. In terms of the photopolymerized hydrogels, the cross-linking degree is directly proportional to the exposure dosage, which refers to the laser energy received by unit volume at unit time. Therefore, the deformation of laser-fabricated structures can be regulated by controlling the exposure dosage. This parameter is primarily influenced by three factors: laser power, exposure time, and the step between scanning points. To simplify experimental procedures and avoid repetitive adjustments of exposure power and time, we exploit the effects of the scanning point step (SPS) to control the exposure dosage and further realize the manipulation of hydrogel deformability. Here, the relative contraction ratio is employed to measure deformation performance. Assuming the length of hydrogel microstructures is $L_{expansion}$ in an expanded state and $L_{contraction}$ in the state of contraction, the relative contraction ratio can be defined as:

$$\alpha = \frac{L_{expansion} - L_{contraction}}{L_{expansion}} \quad (1)$$

The relative contraction ratio reflects the structure's relative deformability. The laser power of 40 mW and a single-point exposure time of 1 ms are employed to fabricate hydrogel disc structures with variable SPSs ranging from 250 to 500 nm (Figure 1e).

 © 2024 Wiley-VCH GmbH

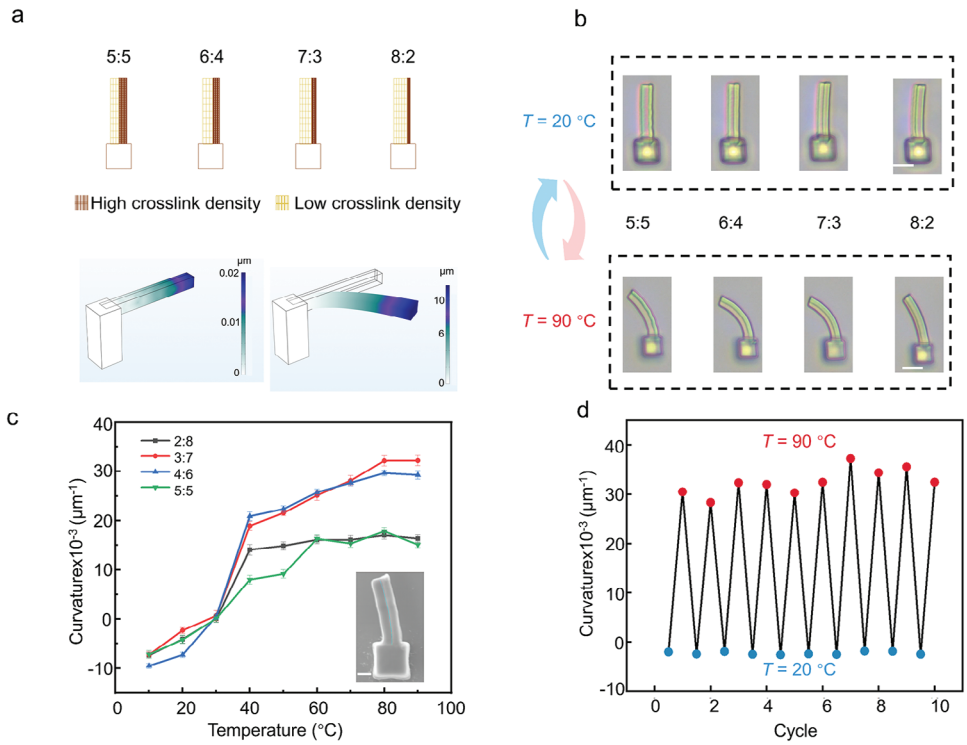

Figure 2. Effects of asymmetric cross-linking density ratios on structural deformation. a) Schematic and stimulation diagrams of asymmetric cross-linking structures. The cross-linking densities of two areas are highlighted in light color and dark color respectively. Light color represents low cross-linking density and dark color represents high cross-linking density. b) Optical schematic diagram of bending deformation of cantilever with different cross-linking ratios at 20 and 90 °C. c) Influence of temperature and cross-linking ratios on cantilever bending curvature. d) A cantilever with a cross-linking ratio of 7:3 on both sides has been selected for the repetitive experiment. Scale bars: b) 10 μm, c) 4 μm.

As the SPS increases, the relative contraction ratio always scales up. When the SPS is less than or equal to 250 nm, the disc hardly shrinks via heating. At an SPS of 500 nm, the relative contraction ratio reaches its maximum value of 51.1%. However, when the SPS is >500 nm, it is exceptionally challenging to cure the hydrogel and complete the process of self-assembly.

For the purpose of broadening potential applications of fs-laser-induced structures, it is crucial to ensure the stability of hydrogel's reversible deformation. Therefore, we have conducted cycle tests on the hydrogel deformation (Figure 1f). During 10 swelling-deswelling processes, the hydrogel exhibits stably switchable deformation, confirming the excellent repeatability of the hydrogel's dynamic response.

The shrinkage induced by heating in the disc structure only enables two-dimensional manipulation, which is unlikely to achieve more complex operations such as rotation, folding, and so on. As shown in Figure 1e, it can be observed that the relative contraction ratios of structures change with the laser SPS. Within a certain range, a larger SPS results in a higher relative contraction ratio. Due to the high precision and flexibility of fs-laser processing, along with the ability to control single-point exposure dosage, it is possible to achieve structural anisotropic deformation by employing different SPSs at various positions within a complete structure. **Figure** 2a presents a designed model which consists of an upright pillar and a cantilever. The pillar plays a supporting role to prevent adhesion of the substrate to the cantilever from hindering its deformation. The cantilever is divided into two regions: the light-colored region with an SPS of 500 nm, representing a low cross-linking density; and the dark-colored region with an SPS of 250 nm, exhibiting a high cross-linking density. When the ambient temperature exceeds T_C (T_C ≈32 °C), both light-colored and dark-colored regions generate simultaneous contraction. The lower cross-linking density in the light-colored region, which introduces a dominant contraction, leads the cantilever into bending toward the light-colored region. Additionally, numerical calculations and simulations are revealed by COMSOL to analyze the deformation. Details are reported in supplementary materials (Figure S1, Supporting Information).

In order to attain maximum bending curvature, relevant experiments have been carried out for exploration. Through our experiments, it is suggested that cantilever bending degrees are associated with designed asymmetric SPSs on both parts. We have observed that when the SPS is <250 nm, the highly cross-linking hydrogels make it less prone to deform even at a high temperature. Conversely, when the SPS exceeds 500 nm, it is hard to cure the hydrogels due to the insufficient energy density. To achieve greater deformation, we ultimately selected an SPS of 250 nm for the dark region and 500 nm for the light region to process the cantilever. The proportion of dark to light regions also influences bending curvatures of the cantilever, and optical images of relevant experiments are depicted in Figure 2b. It can be observed that when the light region occupies 70% and the dark region occupies 30%, the cantilever bending curvature clearly reaches the

© 2024 Wiley-VCH GmbH

16163028, 2024, 44, Downloaded from https://onlinelibrary.wiley.com/doi/10.1002/adfm.202407232 by University Of Science, Wiley Online Library on [02/01/2025]. See the Terms and Conditions (https://onlinelibrary.wiley.com/terms-and-conditions) on Wiley Online Library for rules of use; OA articles are governed by the applicable Creative Commons License

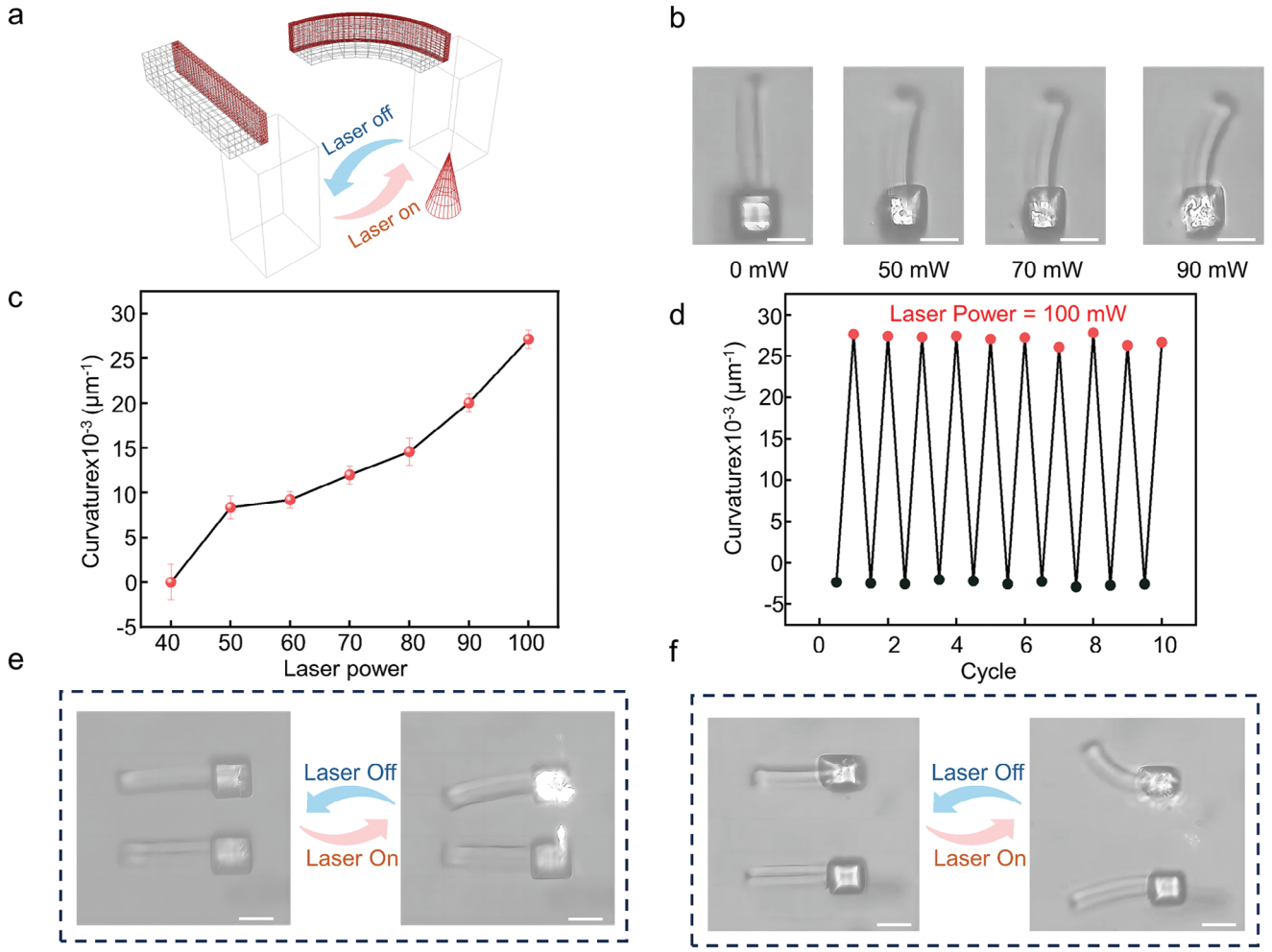

Figure 3. Effects of laser irradiation on structural deformation of thermosensitive hydrogels. a) Schematic diagram of bending curvature of the laser-irradiated cantilever. b) Optical images of cantilever bending deformation affected by variable laser powers. c) Bending curvatures of the cantilever with different laser powers. d) The repetitive experiments of cantilever performances during 10 cycles of laser irradiation. e,f) Two designed mirror symmetrical cantilevers for the control experiment. With one of them irradiated by laser, the other cantilever is also bent under the localized photothermal manipulation. Scale bars: 10 μm.

peak (the bending process is provided in Video S2, Supporting Information).

The cantilever curvature is also related to ambient temperature. We have evaluated the cantilever curvature as a function of temperature (Figure 2c). The radius was obtained by calculating the average curvature of the cantilever with Image J. When the ambient temperature is below T_C ($T_C \approx 32$ °C), the cantilever absorbs water and thus swelling, which causes a unidirectional bending toward the dark region. However, the bending is not pronounced at this temperature. In contrast, when the ambient temperature exceeds T_C, the cantilever bends toward the light region. With an increasing temperature, the bending performance becomes more typical, reaching a stable state at 80 °C.

To assess anti-fatigue effects of the hydrogel, we have conducted repetitive experiments on the cantilever which was fabricated with two SPSs of 500 and 250 nm, accounting for 70% and 30% respectively. The hydrogel has generated multiple cycles of contraction and expansion with the water temperature being altered (20 and 90 °C). The cantilever curvature during this process is measured, confirming the reversibility of the photothermally-responsive hydrogel (Figure 2d).

The expansion and contraction of hydrogels occur in an aqueous environment. Typically, the expansion and contraction processes are manipulated by adding water droplets at different temperatures to the entire structures. However, such method can only globally alter the ambient temperature of the sample, lacking the capability to achieve localized control.

The light regulating method, which features precision, flexibility, and remote controllability, can be leveraged for achieving localized control of photothermally-responsive hydrogels.[16] With a photoinitiator (in this case TPO) in the hydrogel, laser-induced two-photon absorption gives rise to a localized temperature increase, thereby enabling spatially precise localized photothermal regulation of the hydrogel.

As shown in **Figure 3a**, the base connected to the cantilever receives localized heating due to laser irradiation, which is then

© 2024 Wiley-VCH GmbH

16163028, 2024, 44, Downloaded from https://onlinelibrary.wiley.com/doi/10.1002/adfm.202407232 by University Of Science, Wiley Online Library on [02/01/2025]. See the Terms and Conditions (https://onlinelibrary.wiley.com/terms-and-conditions) on Wiley Online Library for rules of use; OA articles are governed by the applicable Creative Commons License

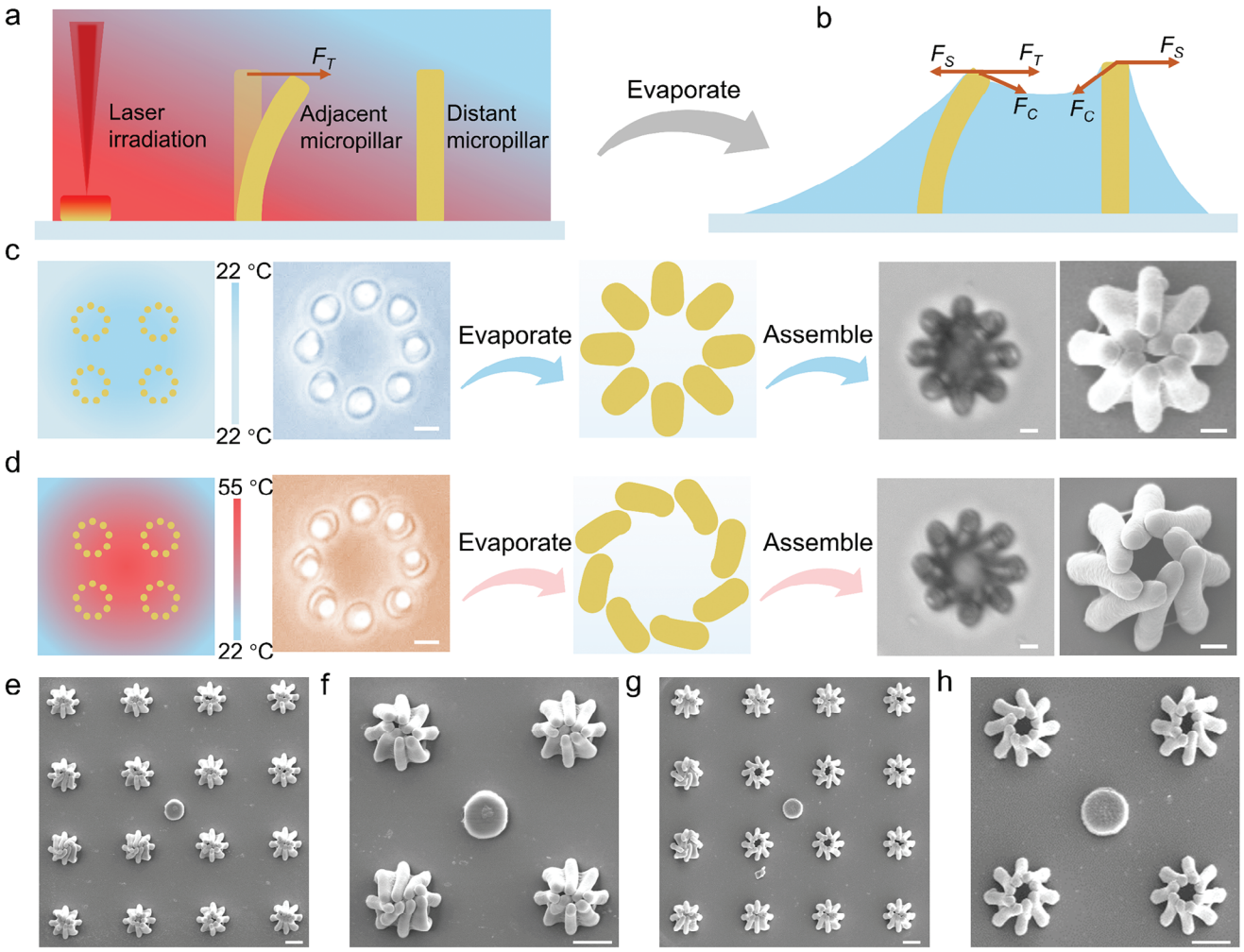

Figure 4. Self-assembly of micropillar arrays with localized photothermal response. a) Schematic diagram of micropillar bending deformation under photothermal effects. With laser irradiating the hydrogel disc, heat is conducted through water, making those closer to the disc bend, while those farther away stay upright. b) Force analysis diagram of micropillars. c) In the condition of water evaporation without light and heat, the micropillars collapse to the middle. d) Under photothermal effects, the micropillars collapse into a chiral structure in the process of water evaporation. e) SEM image of the self-assembled micropillar array without laser irradiation. f) The partially enlarged view of figure e. g) SEM image of the self-assembled chiral array under laser irradiation. h) The partially enlarged view of g). Scale bars:10 µm.

conducted in the vicinity of the cantilever, causing it to generate unidirectional bending. When the laser irradiation ceases, the cantilever restores the original state. We have investigated the impact of laser power on cantilever bending (Figure 3b,c). The experiments have revealed that the cantilever will not bend when the laser power is below 40 mW. As the laser power increases, the bending angle of the cantilever becomes progressively larger, reaching its maximum as the laser power reaches 100 mW. To eliminate the influence of other factors, a controlled experiment is conducted (Figure 3e,f; Video S3, Supporting Information). Two cantilevers have been fabricated with opposite asymmetrical cross-linking ratios so that they will present mirrored bending deformation when subjected to heat. When we apply the laser irradiation to one cantilever, it has bent as expected. What's more, the other cantilever, close to the laser-irradiated one, will also bend due to the influence of laser irradiation. This phenomenon indicates that bending deformation of the cantilever is induced by the photothermal response generated in hydrogel. Furthermore, to validate the feasibility of this approach, repetitive experiments have been performed, and after 10 cycles of laser irradiation, the performance of cantilever bending did not appear significant change (Figure 3d).

Due to the flexibility of fs-laser microfabrication and the programmability of photothermal response, it is of distinctive convenience to construct certain complex chiral structures. By designing various exposure dosages on each part of the hydrogel structure and combining localized photothermal characteristics with CFSA techniques, we have fabricated a locally programmable chiral structure. This work is a breakthrough and of innovations compared to traditional laser-manufactured micro/nano arrays, which can only achieve overall self-assemblies.

According to **Figure 4a**, the micropillar array is placed in water at 20 °C (20 °C < T_C) after photopolymerization and development. Irradiating the truncated cone structure in the middle

© 2024 Wiley-VCH GmbH

16163028, 2024, 44, Downloaded from https://onlinelibrary.wiley.com/doi/10.1002/adfm.202407232 by University Of Science, Wiley Online Library on [02/01/2025]. See the Terms and Conditions (https://onlinelibrary.wiley.com/terms-and-conditions) on Wiley Online Library for rules of use; OA articles are governed by the applicable Creative Commons License

of the array with a fs-laser causes the hydrogel to generate photothermal response. Heat is conducted to the surrounding micropillars, making those closer to the truncated cone bend toward a fixed direction, while those farther away will not present prominent bending deformation (this process is detailed in Video S4, Supporting Information). It is difficult to extract reliable quantitative information about the substrate's temperature distribution based solely on experimental data. Therefore, we conducted a numerical analysis of the 3D heat conduction in the sample to better understand the underlying effects. To address this specific issue in the calculations, we set the temperature of the central hydrogel disc and placed a surrounding water bath to mimic the experimental conditions. To reflect this heat conduction varying with time and space more intuitively, we have performed a temperature field simulation experiment (Figure S2, Supporting Information). As the solution slowly evaporates, the micropillars bend to expected orientation due to the resultant, with Figure 4b as a schematic of each force affecting microstructure units during the assembly. In the temperature field, there are three dominant forces playing roles in the self-assembly process, which are known as the capillary force (F_C), the elastic standing force of micropillars (F_S), and the temperature force (F_T), altering with the ambient temperature. Structures not irradiated by laser or far from the irradiation are mainly affected by F_C and F_S, while structures closer to the laser irradiation position are more susceptible to F_T.

Figure 4c shows the assembly process of micropillars without laser irradiation, where micropillar structures are placed in a 20 °C aqueous solution, with water slowly evaporating. The joint effect of F_C and Fs inward induces the micropillars to collapse toward the center. Once the solution is completely dried, the micropillar tips converge to the center, and the self-assembled structure stays stable under the influence of van der Waals forces. From the SEM images, it is clear that the structure exhibits an achiral state under this circumstance. In Figure 4d, the assembly process of micropillars under laser irradiation is presented. The laser beam is focused on the hydrogel disc in the middle of the array when the aqueous solution is about to evaporate. Due to the anisotropic design of the micropillars, they bend toward the designed direction (counterclockwise) as the temperature rises. When ambient liquid evaporates, as the contact line gradually moves closer to the micropillars, the capillary force generated by the meniscus will amplify this deformation trend, where the resultant of F_C, F_S, and F_T leads the micropillars collapsing toward the tangential direction of the meniscus, inducing a left-handed chiral structure. A simulation experiment was carried out to illustrate such chiral assemblies, detailed in Figure S3 (Supporting information).

Furthermore, to demonstrate the flexibility of fs-laser processing and localized controllability of the photothermal response, a 4 × 4 laser-polymerized micropillar array is presented in Figure 4e, which contains two kinds of structural morphologies (details of tunable self-assemblies are discussed in Figure S4, Supporting Information). In the experiments, the laser-fabricated array was placed in water at 20 °C (20 °C < T_C), and then the hydrogel truncated cone in the middle was irradiated by a fs-laser beam, which brought about photothermal response, and thus passing the heat to the surrounding micropillars, causing those near the truncated cone to bend directionally, while those further away will not show typical changes. Without light irradiation, the micropillars collapse toward the center under the effects of dominant capillary force as the solvent slowly evaporates, not forming chiral structures (Figure 4e,f). Then, by immersing this structure in water, the micropillars can self-unravel to the upright state. With laser irradiation being employed, the joint effects of capillary and thermal forces drive the nearby four micropillar units to assemble into a chiral structure (Figure 4g,h), while the peripheral structures, less affected by heat, do not exhibit chirality after self-assembly. The same assembly morphology can be obtained in the absence of light (Figure S4 and Video S5, Supporting Information). Therefore, through anisotropic design and light regulating, three assembly morphologies (left-handed, right-handed, achiral) are achieved in one array.

In addition, the laser processing power has a significant impact on the self-assembly of micropillar structures. When the laser power is too low (<40 mW), the stiffness of the hydrogel is insufficient so that the entire micropillars collapse randomly after the water naturally evaporates. If the laser power exceeds 55 mW, the hydrogel with strong stiffness almost loses the heat-driven deformability, owing to that the localized controllable bending cannot be realized (Figure S5, Supporting Information).

As a facile and flexible strategy to achieve controllable fabrication of chiral structures, localized light regulating self-assembly presents an effective approach to prepare arrays of distinctive chiral microstructures. In addition, it is of great significance to construct chiral architectures that exhibit chiral optical effects, providing broad prospects for applications in biomolecular detection. The chiral substance recognition based on circularly polarized light, has been widely applied in biology, materials science, and other fields. The chiral optical response arising from the strong interaction between the chiral molecules and circularly polarized light is known as Circular Dichroism (CD). The CD is widely used to detect organic molecules with sizes unambiguously smaller than the wavelength scale, which has been found rare applications in discriminating natural micro/mesoscale chiral structures.

Optical vortices carrying orbital angular momentum (OAM) have been proposed as an exceptional method for detecting the optical chirality of microscopic objects, which is of high flexibility to match the size of the microstructures being detected by adjusting the topological charge. The vortical dichroism (VD) obtains extensive application in optical manipulation, quantum entanglement, nanofabrication, and so on.[32] To characterize the chiral features of self-assembled microstructures, the VD can be calculated using the following formula:

$$VD = 2 \times \frac{I_R - I_L}{I_R + I_L} \tag{2}$$

where I_R and I_L represent the reflection intensities of the chiral microstructures under illumination of right-handed wavefront (RHW) and left-handed wavefront (LHW), respectively. By vertically irradiating the prepared structures with vortex beams of opposite phase fronts, the corresponding reflection intensity spectra can be measured to calculate the VD spectra via the above formula.

© 2024 Wiley-VCH GmbH

16163028, 2024, 44, Downloaded from https://onlinelibrary.wiley.com/doi/10.1002/adfm.202407232 by University Of Science, Wiley Online Library on [02/01/2025]. See the Terms and Conditions (https://onlinelibrary.wiley.com/terms-and-conditions) on Wiley Online Library for rules of use; OA articles are governed by the applicable Creative Commons License

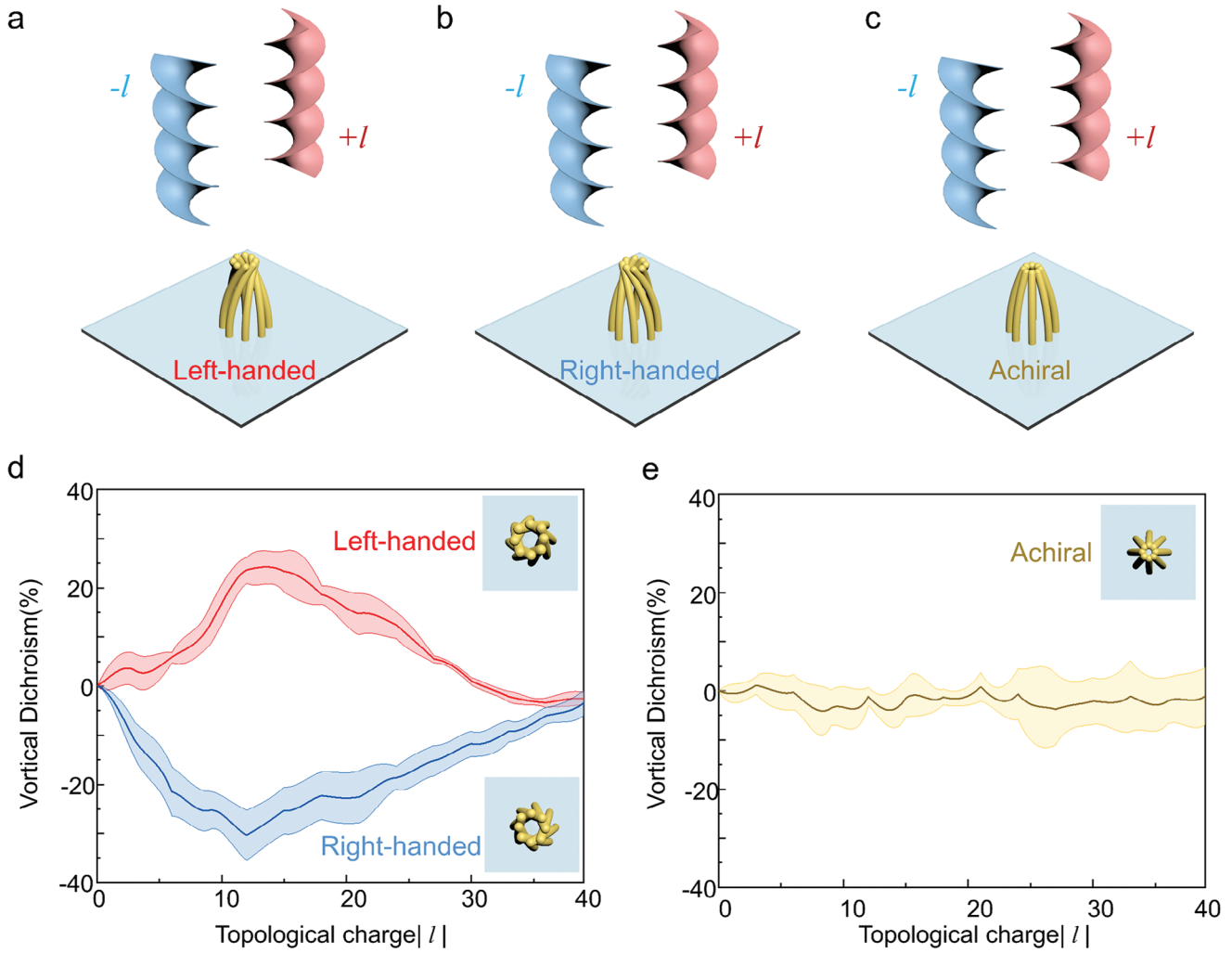

Figure 5. Measured vortical dichroism (VD) of designed microstructures for chiroptical responses. a–c) Schematic diagram of OAM beams vertically irradiated on left-handed a), right-handed b), and achiral microstructures c). d,e) The optical vortical dichroism spectra of chiral d) and achiral e) microstructures.

In the experiments, laser irradiation on the truncated cone structure causes surrounding micropillars to bend directionally. Through the CFSA method, structures with opposite chirality are obtained. After the center of the assembly unit is aligned with the vortex optical axis, vortex beams carrying opposite OAM are vertically irradiated onto the chiral microstructures. Subsequently, the beam diameter is adjusted to approximate the size of structures by changing topological charges. The corresponding VD measurements are performed on left-handed, right-handed, and achiral assemblies successively (**Figure** 5a–c).

VD measurements of chiral self-assembled structures, as shown in Figure 5d,e, have been conducted by placing the structures of opposite chirality under generated vortex beams. With adjusted topological charges, the structures are entirely irradiated by the vortex light. The absolute values of VD initially increase and then decrease (Figure 5d). Figure 5e presents measurements on achiral structures, revealing VD values fluctuating irregularly near the zero-scale line.

It is noteworthy that the VD spectra of opposite chiral microstructures have a slight symmetry error, which is possibly due to inconsistencies in the overall height of the self-assembled microunits along with uneven energy distribution of the probe beam. Compared with the conventional processing methods of chiral structures, we have demonstrated the tunability and localized controllability of prepared chiral microstructures via a light-regulated CFSA method, allowing for efficient and economical fabrication of a large number of microstructures.

3. Conclusion

In conclusion, this paper proposes a method for constructing three-dimensional chiral microstructures through light-regulated CFSA based on photothermally-responsive hydrogels. Exploiting the flexibility of fs-laser printing, asymmetrically cross-linking cantilever structures have been designed to achieve controllable bending. The effects of laser processing parameters, cross-linking ratio, environmental temperature, and laser

© 2024 Wiley-VCH GmbH

16163028, 2024, 44, Downloaded from https://onlinelibrary.wiley.com/doi/10.1002/adfm.202407232 by University Of Science, Wiley Online Library on [02/01/2025]. See the Terms and Conditions (https://onlinelibrary.wiley.com/terms-and-conditions) on Wiley Online Library for rules of use; OA articles are governed by the applicable Creative Commons License

irradiation intensity on the deformation of hydrogels have been thoroughly studied. The conclusions drawn from these experiments have guided subsequent light-regulated self-assembly experiments. With the aid of photothermal response of hydrogels and capillary-force self-assembly, three self-assembled structures (left-handed, right-handed, achiral) are obtained. Analysis of the VD spectra results indicates that light-regulated self-assemblies of photothermally-responsive micropillars possess excellent tunability in chirality. Additionally, differences in vortical dichroism of distinctive self-assemblies have been revealed. This light-regulating strategy based on smart hydrogels unfolds significant possibilities in microstructure fabrication, which holds potential applications in chiral photonics, microsensors, metamaterials, and so on.

4. Experimental Section

Material: The main materials for preparing the photothermally-responsive hydrogel in the experiment involved 400 mg of *N*-isopropylacrylamide, 30 mg of *N,N′*-methylenebis (acrylamide), 30 mg of diphenyl (2,4,6-trimethylbenzoyl) phosphine oxide, and 50 mg of polyvinylpyrrolidone K30, which would be dissolved into 450 µL of ethylene glycol. Additionally, 2 mg of Rhodamine 6G was required for the staining process. All the aforementioned materials were purchased from Aladdin.

Fabrication and Light Regulating Self-Assembly: With a constant temperature and humidity in the laboratory, the ambient temperature was controlled at 20 ± 1 °C, and the humidity was ≈40%. Before laser processing the hydrogel, it was necessary to pipette the hydrogel onto a cover glass which had been treated with the mixture containing 3-methacryloxypropyltrimethoxysilane and methanol with a volume ratio of 1:19 for 12 h. The cover glass should then be placed on a hot plate for baking. This baking step was helpful to reduce the flow of the hydrogel during the subsequent laser processing. Here, the baking time and temperature were 5 min and 90 °C, respectively.

Next, the sample was fixed on the piezoelectric table with controlling the mirror to conduct point-by-point processing through the program. The laser source of the Spectra-Physics MaiTai SP (84 MHz) was used in experiments, with a central wavelength of 800 nm and a pulse duration of 35 fs. Additionally, an oil immersion objective (60×, NA = 1.35, Olympus) was employed to focus the laser beam to alter the polymerization degree of the hydrogel. The 3D coordinates generated by MATLAB were imported into the control software system, thus controlling the corresponding processing path. Furthermore, light-responsive operations were also performed using the aforementioned laser processing platform.

Measurement of Vortical Dichroism: Optical vortices were generated through a spatial light modulator (SLM) with a resolution of 1920 × 1080 and pixel pitch of 8 µm. The SLM in reflection mode, could encode computer-generated holograms with 256 grayscales. After aligning the vortex center with chiral microstructures, surface reflection intensity was collected using a CCD camera.

Characterization: SEM images were obtained with scanning electron microscope (EVO18, ZEISS), and optical microscopy images were taken with an inverted microscope. Optical microscopy (DMI 3000 B, Leica) and CCD (WV-BP334, Panasonic) are used to measure VD spectra.

Simulation: The numerical simulations were performed by adopting a finite-element approach using the commercial software COMSOL Multiphysics to solve the linear elastic Cauchy continuum-mechanics equations. Geometrical nonlinearities have been taken into consideration. In the calculation of the cantilever bending deformation, the structures' response to temperature variation was introduced as a volumetric stress. As different hydrogel cross-linking densities produced shrinkage distinction of the designed cantilever, the elastic bending deformation by heat was modeled by applying the anisotropic thermal strain. The proportion of two distinct cross-linking regions is consistent with the cantilever parameters designed by the experiment. In this way, the thermal expansion coefficient between the lower and higher cross-linking parts presents different. In terms of the thermal diffusion calculation, a central disc structure was focused by laser irradiation, with a surrounding water bath at room temperature, and the discretization was set up in an adaptive manner.

Supporting Information

Supporting Information is available from the Wiley Online Library or from the author.

Acknowledgements

This work was supported by the National Key Research and Development Program of China (2021YFF0502700), the National Natural Science Foundation of China (52175396, 62375073, and 62205236), and Research funds of Central Universities of Hefei University of Technology (JZ2022HGPA0312).

Conflict of Interest

The authors declare no conflict of interest.

Author Contributions

D.W., Z.L., Y.H., C.Z., S.W., C.C., Y.Z., and H.X. conceived the idea and developed the theory; J.N., X.L. and H.H. performed the simulations; Z.L., X.L., C.Z., D.P., and R.D. performed the experiments; Z.L., X.L., S.W., and X.L. analyzed the data and wrote the manuscript; D.W., Z.L., Y.H., C.Z., and S.W. supervised the project. All authors discussed the results and commented on the manuscript.

Data Availability Statement

The data that support the findings of this study are available from the corresponding author upon reasonable request.

Keywords

capillary force self-assembly, chiral microstructures, light regulating, two-photon polymerization

Received: April 27, 2024
Revised: June 15, 2024
Published online: July 2, 2024

[1] M.-Q. Zhao, Q. Zhang, G.-L. Tian, F. Wei, *Nanoscale* **2014**, *6*, 9339.
[2] W. Zhou, Y. Li, K. Je, T. Vo, H. Lin, B. E. Partridge, Z. Huang, S. C. Glotzer, C. A. Mirkin, *Science* **2024**, *383*, 312.
[3] A. Cangialosi, C. Yoon, J. Liu, Q. Huang, J. Guo, T. D. Nguyen, D. H. Gracias, R. Schulman, *Science* **2017**, *357*, 1126.
[4] B. Pokroy, S. H. Kang, L. Mahadevan, J. Aizenberg, *Science* **2009**, *323*, 237.
[5] C. Zeng, M. W. Faaborg, A. Sherif, M. J. Falk, R. Hajian, M. Xiao, K. Hartig, Y. Bar-Sinai, M. P. Brenner, V. N. Manoharan, *Nature* **2022**, *611*, 68.

© 2024 Wiley-VCH GmbH

16163028, 2024, 44, Downloaded from https://onlinelibrary.wiley.com/doi/10.1002/adfm.202407232 by University Of Science, Wiley Online Library on [02/01/2025]. See the Terms and Conditions (https://onlinelibrary.wiley.com/terms-and-conditions) on Wiley Online Library for rules of use; OA articles are governed by the applicable Creative Commons License

[6] S. Li, B. Deng, A. Grinthal, A. Schneider-Yamamura, J. Kang, R. S. Martens, C. T. Zhang, J. Li, S. Yu, K. Bertoldi, J. Aizenberg, *Nature* **2021**, *592*, 386.
[7] D. Jin, Q. Chen, T.-Y. Huang, J. Huang, L. Zhang, H. Duan, *Mater. Today* **2020**, *32*, 19.
[8] Y. Zhang, D. Wu, Y. Zhang, Y. Bian, C. Wang, J. Li, J. Chu, Y. Hu, *Int. J. Extreme Manuf.* **2023**, *5*, 042012.
[9] H. Duan, J. K. W. Yang, K. K. Berggren, *Small* **2011**, *7*, 2661.
[10] D. Wu, S.-Z. Wu, S. Zhao, J. Yao, J.-N. Wang, Q.-D. Chen, H.-B. R. Sun, *Small* **2013**, *9*, 760.
[11] Y. Hu, H. Yuan, S. Liu, J. Ni, Z. Lao, C. Xin, D. Pan, Y. Zhang, W. Zhu, J. Li, D. Wu, J. Chu, *Adv. Mater.* **2020**, *32*, 2002356.
[12] Y. Hu, Z. Lao, B. P. Cumming, D. Wu, J. Li, H. Liang, J. Chu, W. Huang, M. Gu, *Proc. Natl. Acad. Sci. USA* **2015**, *112*, 6876.
[13] Z. Lao, D. Pan, H. Yuan, J. Ni, S. Ji, W. Zhu, Y. Hu, J. Li, D. Wu, J. Chu, *ACS Nano* **2018**, *12*, 10142.
[14] Z. Lao, R. Sun, D. Jin, Z. Ren, C. Xin, Y. Zhang, S. Jiang, Y. Zhang, L. Zhang, *Int. J. Extreme Manuf.* **2021**, *3*, 025001.
[15] H. Wu, Y. Chen, W. Xu, C. Xin, T. Wu, W. Feng, H. Yu, C. Chen, S. Jiang, Y. Zhang, X. Wang, M. Duan, C. Zhang, S. Liu, D. Wang, Y. Hu, J. Li, E. Li, H. Wu, J. Chu, D. Wu, *Nat. Commun.* **2023**, *14*, 20.
[16] C. Xin, Z. Ren, L. Zhang, L. Yang, D. Wang, Y. Hu, J. Li, J. Chu, L. Zhang, D. Wu, *Nat. Commun.* **2023**, *14*, 4273.
[17] J.-Y. Wang, F. Jin, X.-Z. Dong, J. Liu, M.-X. Zhou, T. Li, M.-L. Zheng, *Small* **2023**, *19*, 2303166.
[18] D. Wu, C. Ni, Z. Lao, Y. Cao, J. Ni, Z. Ren, S. Liu, Y. Tao, C. Xin, D. Pan, Y. Hu, J. Chu, *ACS Nano* **2023**, *17*, 12820.
[19] B. Liu, B. Dong, C. Xin, C. Chen, L. Zhang, D. Wang, Y. Hu, J. Li, L. Zhang, D. Wu, J. Chu, *Small* **2023**, *19*, 2204630.
[20] Y. Hu, Z. Wang, D. Jin, C. Zhang, R. Sun, Z. Li, K. Hu, J. Ni, Z. Cai, D. Pan, X. Wang, W. Zhu, J. Li, D. Wu, L. Zhang, J. Chu, *Adv. Funct. Mater.* **2020**, *30*, 1907377.
[21] J. E. Park, J. Jeon, S. J. Park, S. Won, Z. Ku, J. J. Wie, *Small* **2020**, *16*, 2070206.
[22] X. Liu, M. Wei, Q. Wang, Y. Tian, J. Han, H. Gu, H. Ding, Q. Chen, K. Zhou, Z. Gu, *Adv. Mater.* **2021**, *33*, 2100332.
[23] Z. Lao, Y. Zheng, Y. Dai, Y. Hu, J. Ni, S. Ji, Z. Cai, Z. J. Smith, J. Li, L. Zhang, D. Wu, J. Chu, *Adv. Funct. Mater.* **2020**, *30*, 1909467.
[24] M. Zhang, A. Pal, X. Lyu, Y. Wu, M. Sitti, *Nat. Mater.* **2024**, *23*, 560.
[25] X. Wu, R. Ehehalt, G. Razinskas, T. Feichtner, J. Qin, B. Hecht, *Nat. Nanotechnol.* **2022**, *17*, 477.
[26] A. Sutton, T. Shirman, J. V. Timonen, G. T. England, P. Kim, M. Kolle, T. Ferrante, L. D. Zarzar, E. Strong, J. Aizenberg, *Nat. Commun.* **2017**, *8*, 14700.
[27] D. Pan, D. Wu, P.-J. Li, S.-Y. Ji, X. Nie, S.-Y. Fan, G.-Y. Chen, C.-C. Zhang, C. Xin, B. Xu, S. Zhu, Z. Cai, Y. Hu, J. Li, J. Chu, *Adv. Funct. Mater.* **2021**, *31*, 2009386.
[28] C. Deng, Y. Liu, X. Fan, B. Jiao, Z. Zhang, M. Zhang, F. Chen, H. Gao, L. Deng, W. Xiong, *Adv. Funct. Mater.* **2023**, *33*, 2211473.
[29] M. Hippler, E. Blasco, J. Qu, M. Tanaka, C. Barner-Kowollik, M. Wegener, M. Bastmeyer, *Nat. Commun.* **2019**, *10*, 232.
[30] L. Tang, L. Wang, X. Yang, Y. Feng, Y. Li, W. Feng, *Prog. Mater. Sci.* **2021**, *115*, 100702.
[31] G. Pasparakis, C. Tsitsilianis, *Polymer* **2020**, *211*, 123146.
[32] J. Ni, C. Wang, C. Zhang, Y. Hu, L. Yang, Z. Lao, B. Xu, J. Li, D. Wu, J. Chu, *Light: Sci. Appl.* **2017**, *6*, 17011.

© 2024 Wiley-VCH GmbH

16163028, 2024, 44, Downloaded from https://onlinelibrary.wiley.com/doi/10.1002/adfm.202407232 by University Of Science, Wiley Online Library on [02/01/2025]. See the Terms and Conditions (https://onlinelibrary.wiley.com/terms-and-conditions) on Wiley Online Library for rules of use; OA articles are governed by the applicable Creative Commons License